# Improving epigenetic clock performance and interpretation with deep learning

**Lucas Paulo de Lima Camillo**[1,*]**, Louis R Lapierre**[2]**, and Ritambhara Singh**[1,3,*]

[1]Department of Computer Science, Brown University, USA

[2]Department of Molecular Biology, Cell Biology and Biochemistry, Brown University, USA

[3]Center for Computational Molecular Biology, Brown University, USA

*Corresponding authors

Several age predictors based on DNA methylation, dubbed epigenetic clocks, have been created in recent years, with the vast majority based on regularized linear regression. This study explores the improvement in the performance and interpretation of epigenetic clocks using deep learning. First, we gathered 143 publicly available data sets from several human tissues to develop AltumAge, a neural network framework that is a highly accurate and precise age predictor. Compared to ElasticNet, AltumAge performs better for within-data set and cross-data set age prediction, being particularly more generalizable in older ages and new tissue types. We then used deep learning interpretation methods to learn which methylation sites contributed to the final model predictions. We observe that while most important CpG sites are linearly related to age, some highly-interacting CpG sites can influence the relevance of such relationships. Using chromatin annotations, we show that the CpG sites with the highest contribution to the model predictions were related to gene regulatory regions in the genome, including proximity to CTCF binding sites. We also found age-related KEGG pathways for genes containing these CpG sites. Lastly, we compared the age acceleration of AltumAge with Horvath's model, showing that our neural network approach predicts higher age acceleration for tumors and for cells that exhibit age-related changes *in vitro*, such as replicative senescence and mitochondrial dysfunction. Altogether, our neural network approach provides significant improvement and flexibility to current epigenetic clocks for both performance and model interpretability.

1      One of the leading challenges in the field of aging research is measuring age accurately. Monitoring healthy

2   individuals for decades to assess whether an intervention affects the aging process is prohibitive in terms of

3   time and funding. The creation of epigenetic clocks, age predictors that use DNA methylation data, has given

4   researchers tools to measure the aging process quantitatively. Moreover, recent works have demonstrated the

5   effectiveness of precise epigenetic editing based on CRISPR with targeted DNA methylation or demethylation

6   [1]. Consequently, epigenetic clocks have the potential of not only measuring aging but also guiding epigenetic

7   interventions.

8      Notably, two of the most well-known predictors are the ones developed by Hannum *et al.* [2] and Horvath

9   [3] in 2013. Hannum *et al.* developed a blood-based epigenetic clock with 71 CpG sites [2]. Then Horvath

10   showed epigenetic clocks could also accurately predict age across tissues, developing a predictor with 353 CpG

11   sites [3]. Horvath's model has been widely used as it is seen as the state-of-the-art pan-tissue epigenetic clock

12   for humans [4–7]. Both of these works used simple regularized linear regression (ElasticNet) for feature selection

13   and prediction [8]. More recent epigenetic clocks that predict mortality also use a linear combination of features

14   [9, 10]. ElasticNet has been widely used to develop epigenetic clocks [2, 3, 9–13]. Nevertheless, simple linear

15   regression tends to display high bias and fails to capture non-linear feature-feature interactions in the data.

16      Interactions among variables can be taken into account by expanding the feature space with feature mul-

17   tiplication. However, incorporating pairwise CpG site interactions is unfeasible given the high dimensionality

18   of the DNA methylation data. For his model, Horvath [3] selected 353 CpG sites out of total 21,368 sites.

19   If the linear regression had taken into account all pairwise interactions, the feature space would grow to over

20   228 million. A large number of features is especially challenging due to the relatively low number of publicly

21   available DNA methylation samples. Given the complexity of the epigenetic regulatory network, it is likely that

22   important interactions among CpG sites are not captured in the current epigenetic clocks developed thus far.

23      Recently, Galkin *et al.* [14] showed that a deep neural network model, DeepMAge, was slightly superior

24   to Horvath's model in blood samples. However, the authors compared Horvath's pan-tissue predictor to a

25   model trained only in blood DNA methylation data. Moreover, there was no in-depth exploration of why their

26   deep learning model outperformed the ElasticNet model. Similarly, Levy *et al.* [15] developed a deep learning

27   framework to work with DNA methylation data that encodes the CpG sites into latent features for downstream

28   analysis. They showed encouraging results for age prediction using a multi-layer perceptron; however, they

29   investigated only one data set obtained from white blood cells. Therefore, currently, our understanding of the

30   advantages of neural networks for this task in a pan-tissue setting is limited.

31      We introduce AltumAge, a deep neural network that uses beta values from 20,318 CpG sites common to the

Illumina 27k, 450k and EPIC arrays for pan-tissue age prediction (summarized in Figure 1a). We hypothesized that a neural network using all available CpG sites would be better suited to predict pan-tissue age using DNA methylation data due to their ability to (1) capture higher-order feature interactions and (2) leverage important information contained in the thousands of CpG sites not selected by ElasticNet models. AltumAge uses multi-layer perceptron layers (similar to [14, 15]) that account for non-linear interactions by combining multiple features into each node of the network. We trained AltumAge on samples from 143 different experiments, which, to our knowledge, is the largest compilation of DNA methylation data sets for human age prediction. The publicly available data were obtained from multiple studies that used Illumina 27k and Illumina 450k arrays.

We show that AltumAge has a significantly lower error for within-data set age prediction, is better able to generalize to new tissue types and older ages for cross-data set settings, and is more resistant to noise than ElasticNet. For inference, we apply the Shapley-value-based interpretation method, called SHAP [16], on AltumAge to determine the contributions of different CpG sites towards age prediction (summarized in Figure 1b). We confirm that the most important CpG sites have complex interactions resulting in non-linear relationships when predicting age. Such interactions may lead to mechanistic hypotheses on how the epigenetic network interacts to drive the aging phenotype. Additionally, we find that the most important CpG sites are proximal to CTCF binding sites. However, CpG sites in known age-related pathways (SIRT, mTOR, and AMPK) do not seem relevant for age prediction. Finally, our downstream analysis reveals that AltumAge predicts higher age for tumors, senescent cells, cells with mitochondrial dysfunction, and cells with high passage numbers than controls. Overall, we show that deep learning can improve both the performance and interpretation over the widely used ElasticNet and present AltumAge as a useful tool for age prediction.

# Results

## Performance Evaluation

## Model selection

Neural networks can capture complex variable interactions when provided with a large number of high-dimensional datasets. We hypothesized that the same would be true for age prediction with DNA methylation data. For comparison, several machine learning models were trained and validated (see Methods and Supplementary Table S1) to pick the best performing models according to median absolute error (MAE) and mean squared error (MSE). Our primary baseline method is the ElasticNet model, a linear model with implementation following Horvath [3]. We also included two traditional machine learning methods that capture non-linear relationships
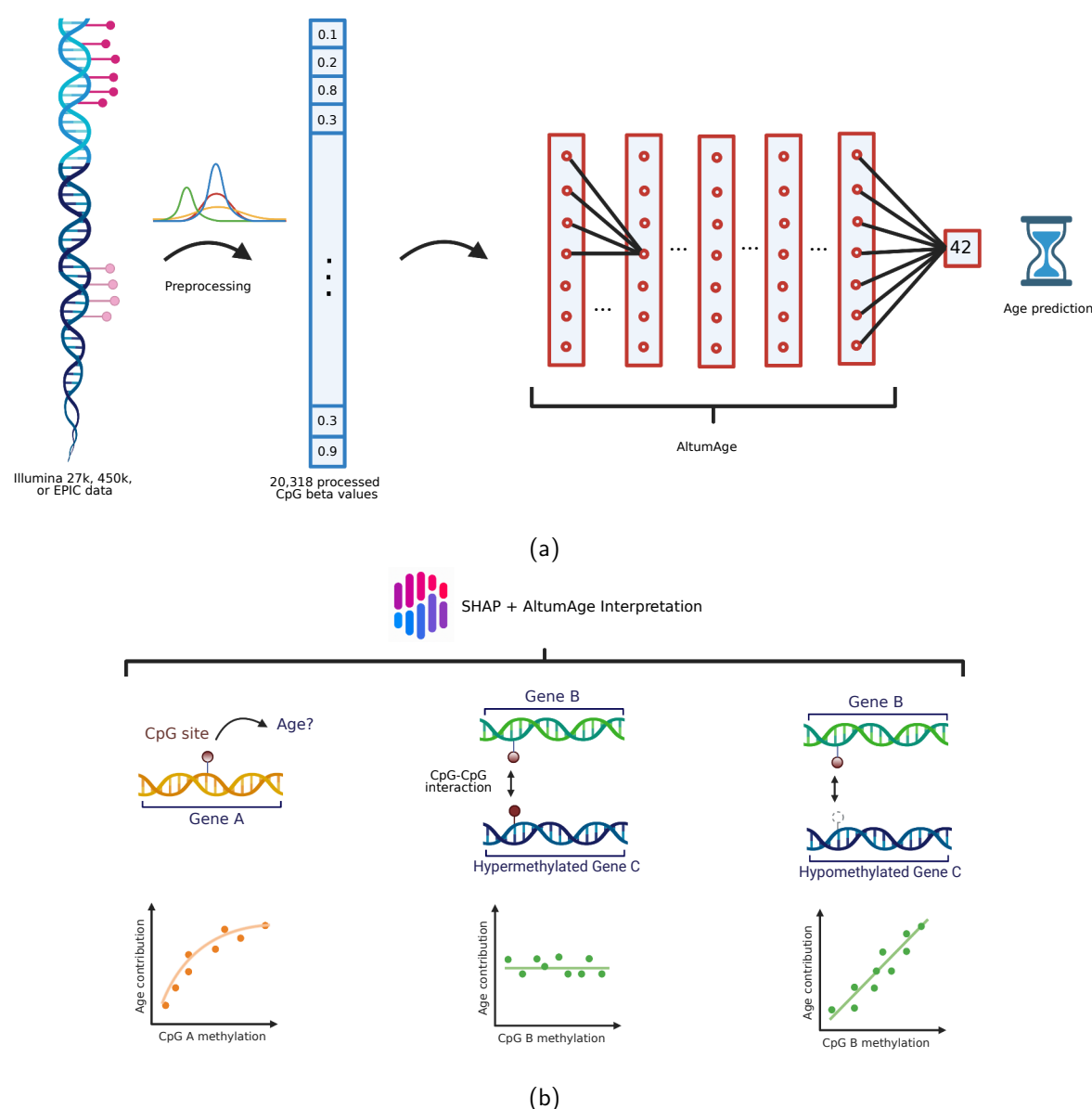
2

Figure 1: AltumAge model and interpretation. (a) DNA methylation data from Illumina 27k, 450k, or EPIC arrays are normalized with BMIQ and scaled. Then 20,318 CpG sites are selected as the input of the model. The information is processed through five hidden layers with 32 nodes each, and the values of the last hidden layer nodes are combined into a single node as the age output in years. (b) For interpretation, a Shapley-values-based method, called SHAP [16], is used to determine how the methylation status of a specific CpG site affects the age output of AltumAge. Relevant CpG sites generally present a primarily linear relationship (left) with the predicted age. However, interacting CpG sites can change such relationships. In some instances, we find that when a secondary CpG site is hypermethylated (middle), the methylation status of the first CpG is irrelevant for age prediction; when it is hypomethylated (right), then the methylation status becomes essential. Images created with Biorender.com.

in the data, random forest and support vector regression; however, they performed poorly on the validation set (MAE = 6.833 and 14.229, respectively). In addition, we tried the neural network TabNet, an attentive interpretable tabular learning method [17], but the error (MAE = 4.172) was slightly worse than the baseline ElasticNet (MAE = 3.674). Lastly, we tuned the hyperparameters of the neural networks based on recent findings that highly regularized deep learning methods excel in tabular data prediction [18]. The best neural

Table 1: Evaluation metrics of AltumAge and different linear models in the test set. The median absolute error (MAE) and the median error are in units of year, while the mean squared error (MSE) is in units of year-squared. Also shown is the number of CpGs whose model importance is greater than zero.

| Model | CpGs | MAE | MSE | R | Median Error |
|---|---|---|---|---|---|
| AltumAge | 20318 | **2.179** | **31.324** | **0.979** | -0.153 |
| AltumAge with ElasticNet CpGs | 1218 | 2.328 | 32.005 | 0.978 | 0.093 |
| AltumAge with Horvath's CpGs | 353 | 2.398 | 32.559 | 0.978 | **0.015** |
| ElasticNet | 1218 | 2.773 | 40.340 | 0.973 | -0.041 |
| Linear Regression with Horvath's CpGs | 353 | 3.247 | 51.628 | 0.965 | -0.025 |
| Horvath's model | 353 | 3.659 | 74.161 | 0.949 | 0.186 |

network model based on both the MAE and mean MSE was dubbed AltumAge (from the Latin *altum*, meaning "deep"). For clarity, a regularized linear regression model with Horvath's age transformation, trained on our 143 data sets, and using the built-in hyperparameter tuning from the Python `glmnet` will be referred to as ElasticNet. On the other hand, the application of Horvath's 2013 epigenetic clock, originally trained on 39 data sets in that paper [3], will be referred to as Horvath's model.

**AltumAge outperforms linear models for within-data set age prediction**

Differences in performance among epigenetic clocks can generally be explained by three factors: the DNA methylation data, the model, and the input CpG sites (or the features). For each of the 143 data sets, we split the total samples - 60% for training and 40% for testing - to avoid introducing any bias in the age, gender, and tissue type distributions. The details of the data sets can be found in the Supplementary Material. We used the same training and test sets for each model to control for the data. Main results are shown in Table 1 and Supplementary Table 3.

We hypothesized that our large and diverse DNA methylation data might improve performance compared to other epigenetic clocks irrespective of model type, adding a confounding variable to any performance improvement seen with AltumAge. To understand the magnitude of such effect, we compared a replication of Horvath's model as seen in [3] with a linear regression trained on our 143 data sets using the same set of 353 CpG sites. Indeed, the regression trained with our data has a lower error (MAE = 3.247 vs. 3.659; MSE = 51.628 vs. 74.161). ElasticNet, with its selected 1218 CpG sites trained with our data, further improves the performance (MAE = 2.773, MSE = 40.340). This result shows that a larger training data set helps the age prediction performance.

Next, we aimed to determine whether the model type, i.e., a linear regression vs. a neural network, would significantly impact the performance. We, therefore, compared the aforementioned linear models with the neural

network AltumAge using the same set of features. AltumAge outperformed the respective linear model with Horvath's 353 CpG sites (MAE = 2.398 vs. 3.247, MSE = 32.559 vs. 51.628) and ElasticNet-selected 1218 CpG sites (MAE = 2.328 vs. 2.773, MSE = 32.005 vs. 40.340). This result shows that AltumAge outperforms linear models given the same training data and set of features.

Lastly, to compare the effect of the different sets of CpG sites, we trained AltumAge with all 20,318 CpG sites available and compared the results from the smaller sets of CpG sites obtained above. There is a gradual improvement in performance for AltumAge by expanding the feature set from Horvath's 353 sites (MAE = 2.398, MSE = 32.559) to 1218 ElasticNet-selected CpG sites (MAE = 2.328, MSE = 32.005) to all 20,318 CpG sites (MAE = 2.179, MSE = 31.324). This result suggests that the expanded feature set helps improve the performance, likely because relevant information in the epigenome is not entirely captured by the CpG sites selected by an ElasticNet model.

Overall, these results indicate that even though more data samples lower the prediction error, AltumAge's performance improvement is far superior to the increased data effect.

A direct comparison of AltumAge and Horvath's model reveals that AltumAge has fewer tissue types with a high MAE. In his 2013 paper, Horvath noticed poor calibration of his model in breast, uterine endometrium, dermal fibroblasts, skeletal muscle, and heart [3]. In our test data, a similarly poor predictive power was found for these tissue types for Horvath's model (breast MAE = 9.462; uterus MAE = 5.798; fibroblast MAE = 10.863; muscle MAE = 9.525; heart not included). AltumAge, on the other hand, had much lower errors for them (MAE = 3.872, 3.049, 5.757, 2.512 respectively). Furthermore, Horvath's model had an MAE > 10 years in 22 tissue types in the test data. AltumAge, on the other hand, had an MAE > 10 in only three tissue types.

Furthermore, Supplementary Figure S1 in particular shows how AltumAge, in contrast to Horvath's model, does not underestimate older ages ( > 60 years) to such an extent (median error = -2.542 vs. -4.651). Better performance in older age is fundamental in defining biomarkers of age-related diseases of which age is the biggest risk factor. Horvath's model systematically underestimates such population partly due to CpG saturation (beta value approaching 0 or 1 in certain genomic loci) [19]. Another reason might be the assumption that age-related CpG changes are linearly correlated with age after 20 years of age. AltumAge resolves these two problems by incorporating an expanded feature set and not using any pre-defined age transformation function that might inject bias in the data processing.

Of note, we were unable to compare AltumAge with DeepMAge [14], another deep learning framework. Unfortunately, neither the code for DeepMAge nor a complete description of its architecture is available.

5

Table 2: Leave-one-data-set-out cross validation evaluation metrics for AltumAge and ElasticNet. The median absolute error (MAE) and the median error are in units of year, while the mean squared error (MSE) is in units of year-squared.

| Model | MAE | MSE | R | Median Error |
|---|---|---|---|---|
| AltumAge | **3.578** | **67.329** | **0.955** | **-0.130** |
| ElasticNet | 3.641 | 72.317 | 0.951 | -0.187 |

**AltumAge is more generalizable than ElasticNet in older ages and in non-blood tissue types**

Leave-one-data-set-out cross-validation (LOOCV) provides a way to understand the generalization potential of a model to new unseen data sets. We performed this LOOCV analysis by leaving out the training samples of each data set (out of the 143) during model fitting. Therefore, the model training was performed using the training set of 142 data sets. Next, we evaluated the performance of this model on the test set of the left-out data set. Consequently, we trained 143 different models in total to evaluate the LOOCV performance for all 143 data sets (Figure 2, Table 2).

Since AltumAge uses 20,318 CpG sites, we expected it to be more prone to noise and overfitting than a model with low variance such as ElasticNet, which effectively uses only a subset of CpG sites. Nevertheless, we see that AltumAge performs better than ElasticNet in both MSE (67.329 vs. 72.317) and MAE (MAE = 3.578 vs. 3.641, Wilcoxon signed-rank test p = 0.0036).

Next, we analyzed the results stratified by absolute error, age, data set, and tissue type. Figure 2a shows a scatter plot of the LOOCV absolute error for each sample according to AltumAge and ElasticNet. Points above the black line favor ElasticNet while the opposite favors AltumAge. As shown by the 100-window rolling mean line, for samples with an absolute prediction error > 3.341 years, on average, AltumAge performs better. This observation is particularly apparent for large deviations. This result indicates, alongside the lower MSE, that AltumAge is more resistant to outliers than ElasticNet when generalizing to new samples.

Stratifying the results by age can give insights into particular strengths and weaknesses of each model. For example, while both models capture the age-related epigenetic drift given the correlation between absolute error and age (AltumAge Pearson's R = 0.376; ElasticNet Pearson's R = 0.423), AltumAge performs better on average for samples with age >30 years (Figure 2b). This result suggests that AltumAge better captures epigenetic changes during aging while ElasticNet better understands the developmental epigenome, since epigenetic changes during childhood and puberty are related to development but after they are mostly due to aging [20].

Finally, we analyzed the performance of each model by data set and tissue type. As shown in Figure 2c, AltumAge performs better than ElasticNet in the LOOCV MAE for data sets with a higher error in performance,

143 i.e., that are more challenging to predict. In comparison, ElasticNet is superior for the ones with a lower

144 error. We observe that most data sets with a low MAE are from newborns or blood samples, and the training

145 set is skewed towards blood-based samples (see Supplementary Figure S2). Therefore, we hypothesized that

146 ElasticNet may be simply performing better for overrepresented tissue types in the training set. To check this,

147 we looked at tissue types for which ElasticNet had a 50% worse LOOCV MAE than AltumAge (capturing a

148 large deviation) and vice versa. As expected, ElasticNet does not generalize as well to a large variety of tissue

149 types (Figure 2d). At the same time, it performs better in blood-based samples (Figure 2e). These observations

150 imply that AltumAge can better generalize to more tissue types, likely capturing global age-related epigenetic

151 patterns, while ElasticNet could be focusing primarily on blood changes.

152 As each model has its benefits and drawbacks, we checked the performance of an ensemble of both methods.

153 Interestingly, we observe a substantial decrease in both MAE (3.269) and MSE (61.962) by averaging the

154 predictions of both models. These results indicate that combining deep learning and linear model predictions

155 may further improve the age prediction performance.

**AltumAge is more robust to noise than ElasticNet**

157 Another desired property of epigenetic clocks is reliability. Noise derived from the experimental procedure,

158 biological or technical replicates may negatively influence the model's reliability. AltumAge was trained with

159 Gaussian noise and adversarial regularization to be more robust against random variation [21]. Gaussian noise

160 introduces normally distributed fluctuations in between hidden layers. Adversarial regularization includes artificial

161 observations with subtle modifications in the loss function that attempt to fool the model into increasing the

162 error. To assess the robustness of AltumAge and ElasticNet to noise, we gradually added artificial Gaussian

163 noise in the beta value of each CpG site up to one standard deviation in the within-data test set and tracked

164 MAE (Figure 3a) and MSE (Figures 3b). As expected, the error grows much faster in the ElasticNet model,

165 particularly with the MSE, which is more swayed by outliers.

166 Furthermore, we examined a new independent whole blood data set GSE55763 (not used in training or

167 testing), which contains 2 technical replicates for each of its 36 samples. Ideally, the difference in prediction

168 between the replicates would be zero. As shown in the histogram in Figure 3c, the median absolute difference for

169 AltumAge is 1.516 years, whereas for ElasticNet, 1.845 years, while the maximum absolute difference is 3.597

170 and 6.654 years, respectively. Despite no significant difference in distributions — likely due to the small sample

171 size — the models differ in whether they capture an artifact effect between replicates. As anticipated, we do

172 not observe a statistically significant effect from replicate one to two for AltumAge (linear mixed-effects $p =$
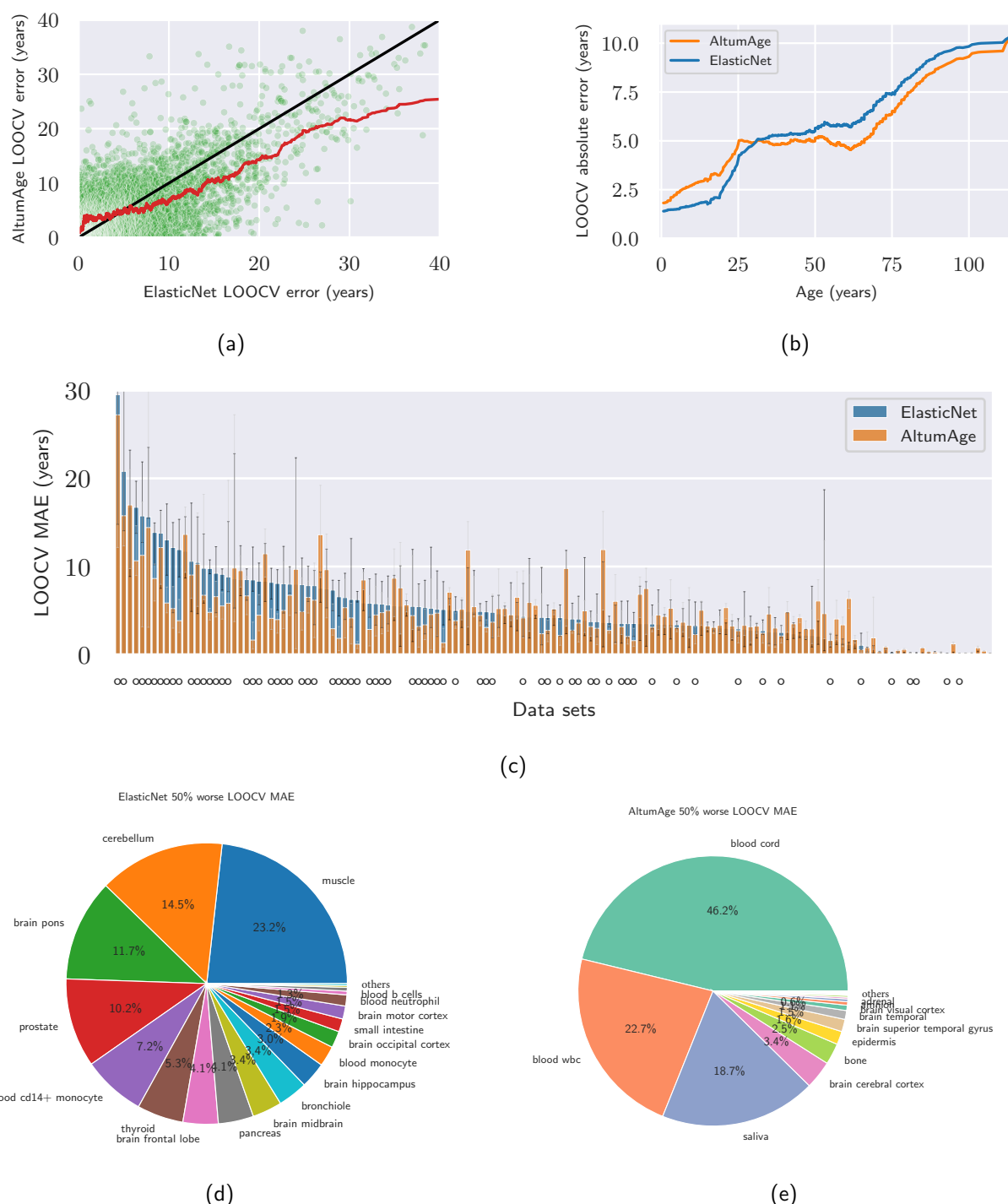
Figure 2: Comparison of leave-one-data-set-out cross-validation (LOOCV) performance between AltumAge and ElasticNet. (a) Scatter plot contrasting the LOOCV absolute error of each model by sample. The black line separates the region in the graph in which AltumAge performs better (bottom right) versus where ElasticNet is superior (top left), and the red line is a 100-sample rolling mean. AltumAge outperforms ElasticNet, particularly in difficult-to-predict tissue types. (b) The 1000-sample rolling mean of the LOOCV absolute error of each model by age. AltumAge has a lower absolute error for age >30 years on average. (c) Bar plot showing the LOOCV median absolute error (MAE) by data set for each model, with 95% confidence interval error bars calculated from 1000 bootstrap iterations. A circle below a bar represents data sets in which AltumAge had a lower LOOCV MAE than ElasticNet. (d) Pie plot showing which tissue types ElasticNet had at least a 50% worse MAE than AltumAge. (e) Pie plot with the converse. Overall, AltumAge can better generalize to more tissue types, whereas most of the improved ElasticNet performance comes from blood-based tissues.

173 0.441). However, we see that ElasticNet predicted a slightly higher age of 0.848 years for replicate two (linear

174 mixed-effects p = 0.031). Overall, the results highlight that resistance to random noise may help in real-world

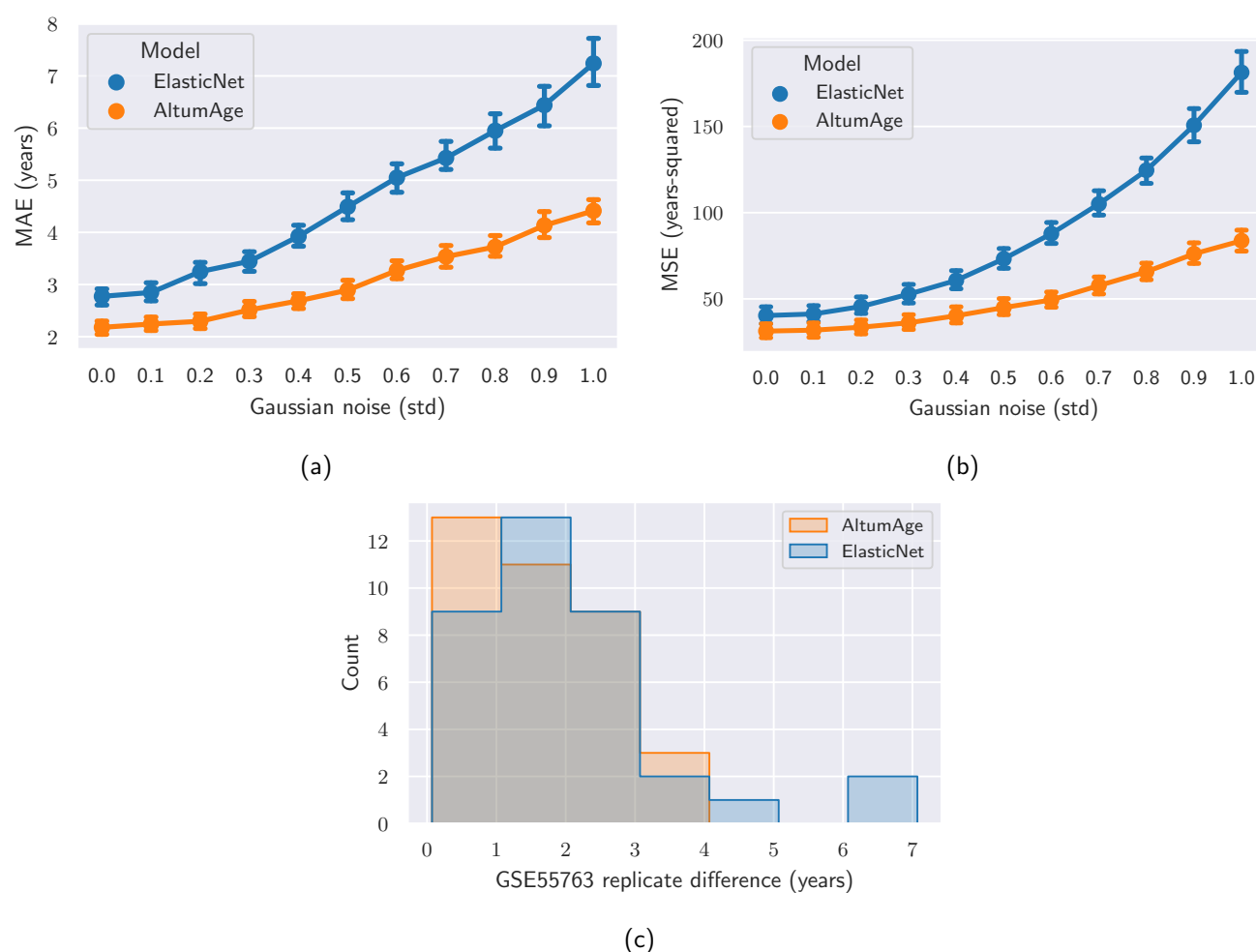175 scenarios, increasing model robustness and reliability.



(a)

(b)

(c)

Figure 3: Comparison of resistance to noise between AltumAge and ElasticNet. (a, b) Point plots show the increase in median absolute error (MAE) and mean squared error (MSE) per model when adding artificial Gaussian noise of up to one standard deviation for each feature. AltumAge is more resistant to noise in both metrics. Shown are the 99% confidence interval error bars calculated from 1000 bootstrap iterations. (c) Histogram of the difference in predicted age between two technical replicates in an independent whole blood data set (GSE55763). AltumAge has a lower median and maximum deviations than ElasticNet.

**Inference**

177 Neural networks, particularly in the context of deep learning, used to be seen as "black-box" methods, as their

178 interpretability was difficult. On the other hand, regardless of the predictive power of ElasticNet models, they

179 are easily understandable. Recently, various methods have been proposed to extract the contribution of features

180 towards prediction in neural networks. They include interpretation based on model gradients [22–24], attention

181 [25], among others. One such inference method is SHAP [16], which uses a game-theoretic approach to aid

in the explanation of machine learning methods. It can measure how one feature contributes to the output of deep neural networks. For our case, the SHAP value can be conceived as how much the value of one CpG site affects the age output of the model in years. Through the architecture of neural networks, it can also determine which CpG sites most highly interact with each other.

We present results for model inference using SHAP that assist with understanding AltumAge. To support the results obtained by SHAP, we also applied another method of determining feature importance called DeepPINK [26] (see Supplementary Information).

**AltumAge captures relevant age-related CpG-CpG interactions**

Epigenetic modifications can significantly influence gene expression. They can also impact genes that affect other epigenetic changes. Therefore, some CpG sites interact with others through the gene expression network and can work in tandem. Through SHAP, we show that AltumAge can measure how hyper- or hypomethylation of secondary CpG sites affects the relationship of a CpG of interest and age. Supplementary Figure S7 shows scatter plots of the nine most important CpG sites based on SHAP-based importance values assigned to the CpG sites of the samples in the test set. These nine CpG sites account for 1.99% of the total model importance (Supplementary Figure S3). The dependence plots show both the relationship of a CpG site with the predicted age and how that relationship can be affected by the value of a secondary CpG site for a DNA methylation sample. This secondary CpG site has the highest interaction with the CpG of interest, as determined by SHAP values. One way to understand the effect of the secondary CpG site is to focus on the samples in the top and bottom deciles of its methylation value, looking for any differences that may arise due to hyper- or hypomethylation respectively. We uncovered three different types of relationships between CpG site methylation value and age: (1) completely linear, which are independent of CpG-CpG interactions; (2) bivalently linear, whose slope is dependent on a secondary CpG site; and (3) non-linear, affected by a secondary CpG site.

Out of the top nine CpG sites, only cg04084157 (Figure 4a), the fifth most important, shows a completely linear relationship. We subdivided the samples in the test set into the top and bottom deciles for cg07388493, the most highly interacting CpG site. Both subsets display linear relationships (Figure 4b) with indistinguishable regression coefficients (Z-test [1] p = 0.346). Consequently, we observe that the effect of cg04084157 on the age output is independent of the value of the most highly interacting CpG site, cg07388493.

The effect of cg10523019 (Figure 4c), the seventh most important CpG site, displays a bivalently linear rela-tionship. The regression coefficient when cg01511567, the most highly interacting CpG site, is hypomethylated

---

[1] $z = (coef_1 - coef_2)/\sqrt{sd_1^2 + sd_2^2}$, here $coef$ is the coefficient, $sd$ is the standard deviation

10

211 (coef $= 0.539$) is more than twice when it is hypermethylated (coef $= 0.262$, Z-test p $=$ 6.3e-238, Figure 4d).

212 This dual response may also shine a light on relevant age-related biological processes. cg01511567 is located

213 in the gene SSRP1, a subunit of the chromatin transcriptional elongation factor FACT, and cg10523019 lies in

214 RHBDD1, a gene involved in proteolysis and apoptosis. Since RHBDD1 has a long transcript of 163,280 base

215 pairs (about seven times the median gene length [27]), FACT likely aids RHBDD1's transcription. When SSRP1

216 is expressed (with cg01511567 hypomethylated), RHBDD1 has more influence on age prediction. However, if

217 SSRP1 is repressed (with cg01511567 hypermethylated), the methylation status of cg10523019 becomes less

218 relevant as transcription of RHBDD1 may become deficient due to lack of SSRP1. Laboratory experiments

219 would have to be performed to more thoroughly characterize these relationships; however, it is possible to

220 obtain data-driven hypotheses from these dependence plots.

221 An example of a non-linear CpG-age relationship comes from the top most important CpG cg22736354

222 (Figure 4e). When cg02153528, the most highly interacting CpG site is hypomethylated, the relationship between

223 cg22736354 and age output is still linear, despite its heteroscedasticity (or unequal scatter). However, when

224 it is hypermethylated, it becomes non-linear (Figure 4f). While Pearson's correlation coefficient for a straight

225 line is high (0.892), the residual plot (Supplementary Figure S8) shows underestimation at the boundaries with

226 overestimation in the center. This pattern demonstrates non-linearity; a cubic regression corrects the bias of

227 under and overestimation and increases the correlation coefficient to 0.947. Overall, our results using SHAP

228 values demonstrate that AltumAge captures the non-linear interaction between CpG sites.

229 Note that despite their important effects on the predicted age, some of the CpG sites that interact with

230 the most important CpG sites may themselves not be particularly relevant for the output. For example, the

231 aforementioned cg02153528, the CpG with the highest interaction with the most important CpG site, ranks 11052

232 and 14928 according to SHAP and DeepPINK, respectively, out of 20,318. These results suggest that ElasticNet

233 may miss DNA loci that regulate other loci in aging, and this may partly explain AltumAge's performance

234 improvement compared to ElasticNet.

235 **Characterization of CpG sites by model interpretation**

236 CCCTC-Binding factor (CTCF) is a transcription factor involved in the negative regulation of several cellular

237 processes. It also contributes to long-range DNA interactions by affecting chromatin architecture. We examined

238 whether CpG sites with a higher SHAP importance were closer to CTCF binding sites. The 353 important CpG

239 sites selected by Horvath's model were not closer to the CTCF binding sites when compared to the 21,368 control

240 CpG sites from which the paper's ElasticNet model was trained (Mann-Whitney U-test p-value $= 0.991$). As

11

Figure 4: Three main types of relationship between the scaled beta value of a CpG site and age according to SHAP. Dependence plots of the fifth (a), seventh (c), and first (e) most important CpG sites exemplify the three types of relationship. Samples into the top (red) and bottom (blue) deciles of the most highly interacting CpG site were divided, representing hyper- and hypomethylation respectively. The relationshps are completely linear (b), bivalently linear (d), and non-linear (f). Regression lines are shown in (b), (d), and (f) with a 95% confidence interval calculated from 1000 bootstrap iterations. A cubic regression is also shown in (f) to demonstrate the better fit of the non-linear model.

for AltumAge, since it uses all of the 20,318 CpG sites as features, we compared the top 1000 CpG sites to the control, as the ElasticNet model applied on the full data set selects $1218$ sites as important. These sites comprise 50.8% of SHAP importance. In line with previous studies [28–30], we find that the selected important CpG sites are overwhelmingly closer to CTCF binding sites (Mann-Whitney U-test p-value $= 0.00636$, Supplementary Figure S4). This observation suggests that epigenetic alterations proximal to such loci that are involved in chromatin packing by affecting CTCF binding may be captured by AltumAge. This result is relevant because chromatin structure modifications have been associated with aging (see review [31]).

Due to the close relationship between chromatin and aging, we hypothesized that different chromatin states would influence the importance of each CpG site. ChromHMM is a Hidden Markov Model used for the characterization of chromatin states [32]. Annotations for several cell lines and tissue types are widely available online. Since AltumAge is a pan-tissue epigenetic clock, we used the mode of the 18-state annotation from 41 different tissues obtained from ENCODE for each CpG location [33] (Supplementary Figure S5, Supplementary Table S2). CpG SHAP importance values are indeed impacted by ChromHMM state (Kruskal-Wallis H-test p-value = 5.756e-22). The chromatin state with the highest SHAP normalized median importance was a genic enhancer (SHAP importance = 9.45e-10%, top 69th percentile of all CpG sites). This result supports the idea that some enhancers might be highly relevant to aging [34]. Of note, the chromatin state with the highest DeepPINK normalized median importance was heterochromatin (DeepPINK importance = 2.47e-14%, top 66th percentile of all CpG sites).

**Aging-related pathways**

One of the main interpretation advantages of AltumAge compared to ElasticNet is that the former effectively uses a much larger feature space. CpG sites in aging-related genes are often not selected within the couple hundred features of an ElasticNet model, thus making analyses of these CpG sites of interest impossible. AltumAge allows a closer look at the relationship of CpG sites in aging-related pathways even when these CpG sites are not particularly important for the final age prediction. It is worth analyzing the relative importance of CpG sites in well-known age-related pathways such as SIRT, mTOR, and AMPK [35–37].

Unexpectedly, most of the CpG sites in SIRT genes do not appear relevant, at least directly, for age prediction using AltumAge. Located in SIRT2, cg27442349, accounting for 0.0389% of the total SHAP importance and ranked 574, has the highest SIRT SHAP importance value (Supplementary Figure S6). Other SIRT CpG sites were much below rank 1000.

Out of the 67 proteins participating in the mTOR signaling pathway according to the PID Pathways data set [38], cg11299964, located in MAPKAP1, has the highest SHAP importance of 0.075%, ranking 119. Surprisingly, mTOR was not particularly relevant, with its most important CpG site being cg07029998 (SHAP importance = 0.022%, rank 1544) (Supplementary Figure S6).

In terms of the AMPK pathway, out of CpG sites in genes for the proteins that directly activate or inhibit AMPK from the KEGG database [39], cg22461835, located in ADRA1A, has the highest SHAP importance of 0.093%, ranking 69 (Supplementary Figure S6). Most, however, ranked below 1000.

We also performed KEGG pathway analysis on the genes related to the top-ranking nine CpG sites using

13

KEGGMapper [40]. We found the following genes associated with four of them - NHLRC1, involved in proteolysis; EDARADD, involved in NF-kappa B signaling pathway; NDUFS5, involved in metabolic pathways, including oxidative phosphorylation and thermogenesis; and FZD9, involved in a range of age-related diseases, including cancer and neurodegeneration. Note that DNA methylation affects gene expression depending on its position. A methylated CpG site in an enhancer, promoter, or gene body may impact gene regulation differently. These findings show how methylation in specific loci in aging-related pathways can contribute to age prediction. This insight may not be possible to obtain using ElasticNet due to its focus on selecting only the most important CpG sites related to aging. For example, only cg11299964 (from MAPKAP1 mentioned above) was present among the 353 sites selected by Horvath's model.

## Biological applications

The age acceleration, defined as the predicted age minus the real age, of epigenetic clocks have been shown to be related to several biologically relevant events and characteristics, such as obesity [41], menopause [42], diet [43], heart disease [44], anxiety [45], and even socioeconomic status [46], among others. Since most of these studies have used Horvath's model, we compared AltumAge with Horvath's model to assess the biological significance of AltumAge's age acceleration.

## AltumAge predicts higher age acceleration for cancer

Cancer cells display several genetic and epigenetic aberrations which have been related to aging and mortality by epigenetic clocks [47–49]. Liu et al. [50] have reported that some age predictors consistently estimate higher age acceleration for tumors, whereas others show tissue-specific behavior. Therefore, we examined the age acceleration of cancer samples from 14 data sets comprising 10 tissue types in total for AltumAge, using Horvath's model as a benchmark (Figure 5). Overall, Horvath's model was not able to differentiate between normal and tumor samples (Mann-Whitney U-test p-value = 0.135, Figure 5a). Its median age acceleration for cancer was higher in five tissue types and lower in another five. AltumAge, in contrast, predicts overall higher age acceleration for cancer when compared to normal tissue by 4.832 years (Mann-Whitney U-test p-value = 1.55e-17, Figure 5b). The only two tissue types in which AltumAge estimates a slightly lower age acceleration for cancer are colon and nasopharyngeal tumors, possibly due to their smaller samples size.
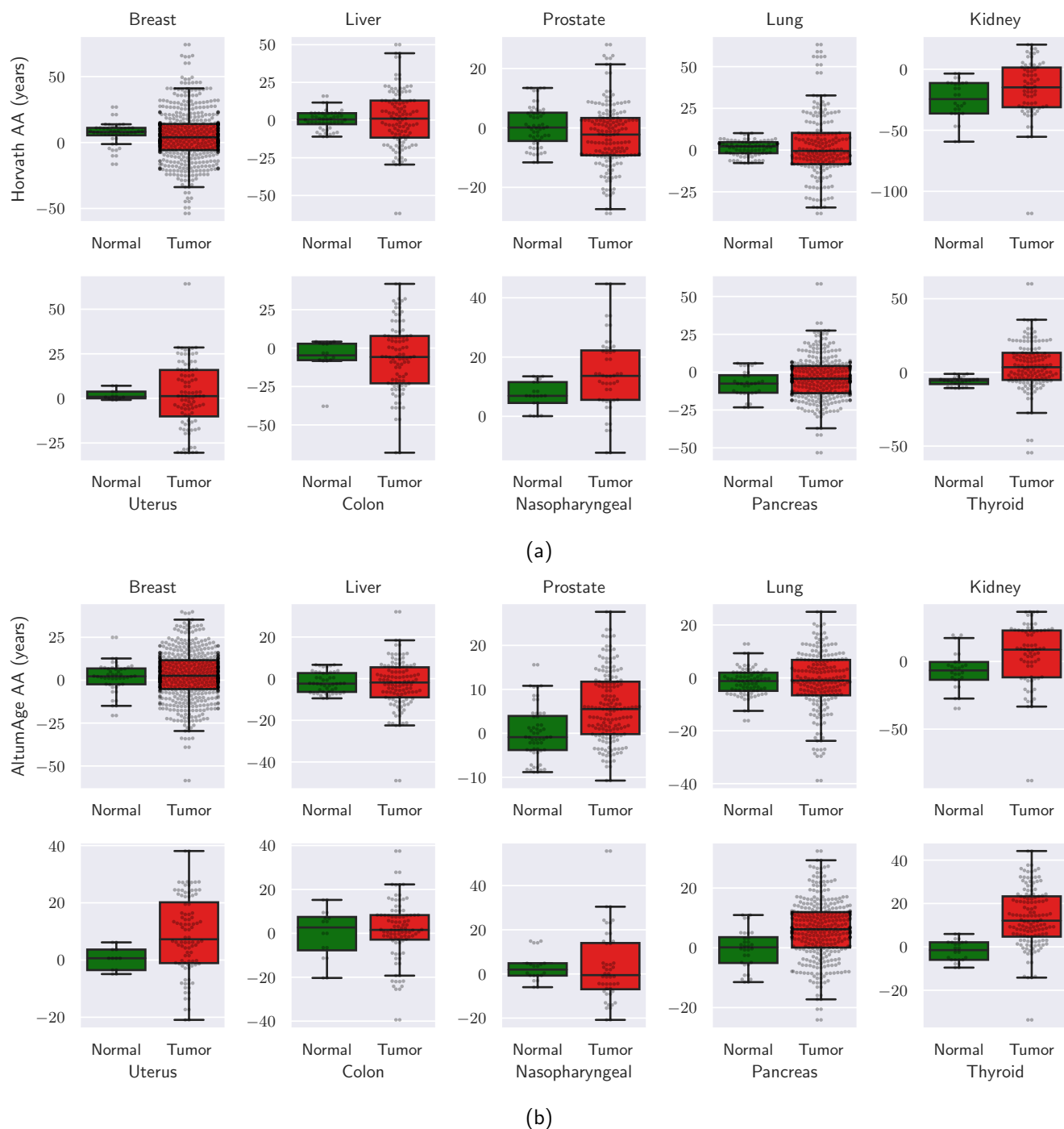
14

Figure 5: Box plots showing age acceleration (AA) in normal and cancerous samples by tissue type according to Horvath's model (a) and AltumAge (b). Horvath's model does not consistently predict higher AA for cancer, with tissue-specific behavior. On the other hand, AltumAge generally predicts higher AA for tumors in all but two cancer tissue types with the two lowest sample numbers (colon and nasopharyngeal).

## AltumAge in vitro age prediction

To assess whether AltumAge can capture biologically relevant changes *in vitro*, we examined independent data sets (not used for training or testing) to understand the effect of cellular senescence, cell passage number,

15

307  mitochondrial depletion, NLRP7 knockdown, and transient cellular reprogramming. We compared AltumAge

308  with Horvath's model as a benchmark.

309  Cellular senescence is a well-known hallmark of aging. A study (with accession ID GSE91069 [51]) provides

310  methylation data from cultured fibroblasts in early passage (EP), near senescence (NS), oncogene-induced

311  senescence (OIS), and replicative senescence (RS). Despite the small sample size (n = 15), AltumAge displays

312  a sequential increase in median predicted age going from EP to NS to OIS to RS (Figure 6a). We observe

313  an increase between EP and RS (one-sided Mann-Whitney U-test p-value = 0.047). Horvath's model also

314  captures a sequential increase from EP to NS to RS, although with lower confidence in differentiating EP from

315  RS (one-sided Mann-Whitney U-test p-value = 0.131).

316  Given that AltumAge detects a tentative link between replicative senescence and higher age, we looked into

317  a study (with accession ID GSE30653 [52]) which contains information of induced pluripotent stem cells (iPSCs)

318  and embryonic stem cells (ESCs) by passage number. We observe that AltumAge detects a strong correlation

319  (Pearson's R = 0.436, p-value = 3.187e-09) between the predicted age and the passage number. As shown

320  by Figure 6c, cells begin with a slightly negative age that increases markedly as they are passaged. Horvath's

321  model also detects a significant correlation (Pearson's R = 0.273, p-value = 3.245e-04), albeit it is weaker when

322  compared to AltumAge. The increase in age with passage number is also much more subtle. The suggestive

323  difference in cultured fibroblasts from EP to RS in addition to the relatively large effect of passage number on

324  predicted age indicates that AltumAge is sensitive to replicative senescence.

325  Mitochondrial dysfunction is another important hallmark of aging. A study (with accession ID GSE100249

326  [53]) contains data on 143B cells chronically depleted of mitochondrial DNA (rho0-). Both AltumAge and

327  Horvath's model predict a higher age for cells with mitochondrial dysfunction (one-sided Mann-Whitney U-test

328  p-value = 0.050, Figure 6d).

329  The NLRP gene family of receptors, primarily expressed in immune cells, is involved in the normal response

330  to inflammation. Mutations in some of these genes are involved in immune system malfunction, excessive

331  inflammation, and disease [54–56], suggesting it may also have ramifications in aging. Moreover, cells with

332  NLRP7 knockdown display aberrant CpG methylation patterns [57]. We, therefore, analyzed DNA methylation

333  data from H9 ESCs (accession ID GSE45727 [57]) with or without NLRP7 knockdown. AltumAge and Horvath's

334  model predict a higher age for knockdown cells (one-sided Mann-Whitney U-test p-value = 0.050, Figure 6e).

335  When H9 cells are exposed to BMP4 differentiating medium, AltumAge is still able to capture the increase in age

336  (one-sided Mann-Whitney U-test p-value = 0.050), while Horvath's not as confidently (one-sided Mann-Whitney

337  U-test p-value = 0.100, Supplementary Figure S9).

338      Lastly, we investigated whether AltumAge could capture a rejuvenation event caused by transient expression
339 of several reprogramming factors in aged human fibroblasts and endothelial cells (GSE142439) [58]. Sarkar
340 et al. [58] demonstrated that several biomarkers such as H3K9me3, SIRT1, HP1$\gamma$, and $\beta$-galactosidase were
341 restored to a youthful state after treatment. Horvath's model was able to capture a decrease in epigenetic
342 age (linear mixed-effects model p-value = 0.004, Figure 6b). Interestingly, there was no difference before and
343 after the intervention according to AltumAge (linear mixed-effects model p-value = 0.845, Figure 6b). While
344 the researchers tracked the cells until six days after treatment, it is possible that the apparent restoration of
345 youthful biomarkers would not endure. Indeed, studies have shown that transient reprogramming causes only
346 temporary rejuvenation [59–61]. Altogether, AltumAge captures an expanded global methylation landscape and
347 can robustly recognize age-related epigenetic patterns while avoiding overestimating the impact of temporary
348 interventions.

## Discussion

350 The creation of new quantitative aging measurements has been rapidly expanding with the burgeoning field of
351 the biology of aging. Epigenetic clocks are a tool that can aid researchers to understand better and to measure
352 the aging process. In 2013, Horvath showed it was possible to use just a couple of CpG sites to predict a person's
353 age based on DNA methylation accurately. It was a giant leap in the field. However, his 2013 ElasticNet model
354 or other versions of linear models are still widespread despite recent advances in machine learning. The accuracy
355 of such linear models was so good that it was difficult to imagine a model significantly outperforming it [62].
356 Other deep learning methods, which slightly outperform ElasticNet, have focused thus far only in a single tissue
357 type [14] [15].

358      We show that our neural network-based model, AltumAge, is an overall better age predictor than ElasticNet.
359 While our more comprehensive and larger data does improve the performance, the capability of neural networks
360 to detect complex CpG-CpG interactions and the expanded feature set with 20,318 CpG sites also contribute
361 to its lower error. For within-data set prediction — which is the case for several studies which create a new
362 epigenetic clock — AltumAge performs drastically better than state-of-the-art methods. Even for LOOCV
363 analysis, while the improved performance of AltumAge over ElasticNet was not as substantial, it performed
364 better in older ages and new tissue types. Arguably, a more generalizable model like AltumAge can better
365 capture pan-tissue age-related changes.

366      Deep learning models have shown promise in several biological tasks, given their good performance on
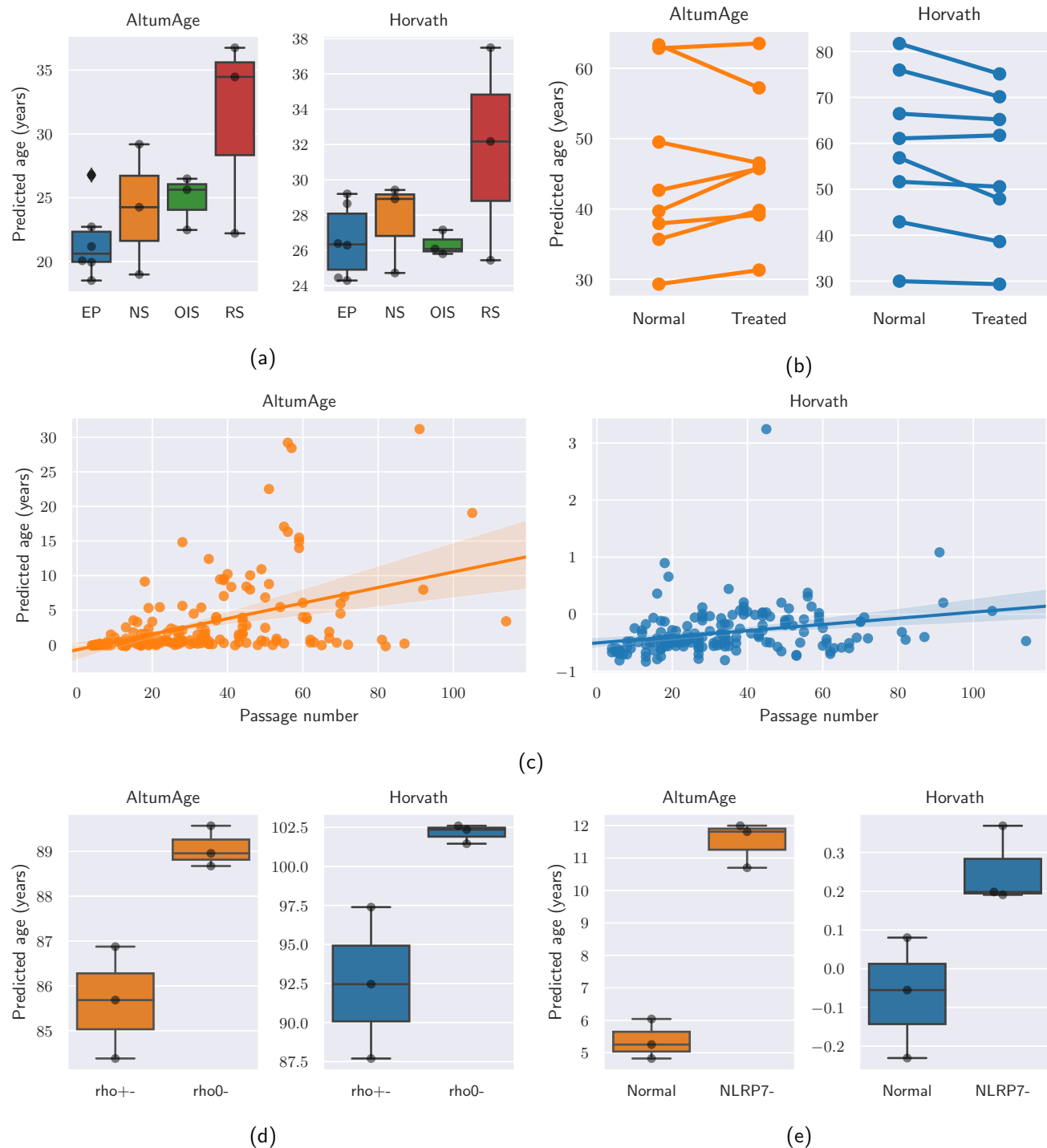367 unstructured data. They have been for many years seen as "black-box" models, but new tools have made it

Figure 6: Analysis of the effect of cellular senescence, cell passage number, mitochondrial depletion, NLRP7 knockdown, and transient cellular reprogramming on predicted age comparing AltumAge and Horvath's model. (a) Box plots showing predicted age for cultured fibroblasts in early passage (EP), near senescence (NS), oncogene-induced senescence (OIS), and replicative senescence (RS). (b) Point plot showing age prediction in human fibroblasts and endothelial cells before and after transient reprogramming. (c) Scatter plot of predicted age of iPSCs and ESCs by passage number with best fit line with 95% confidence interval calculated from 1000 bootstrap iterations. (d) Box plots showing predicted age in 143B cells with mitochondrial depletion (rho0-) or control (rho+-). (e) Box plots showing predicted age of H9 ESCs with NLRP7 knockdown (NLRP7-) or control (Normal).

368    possible to get insights as profound, if not more detailed, than simple ElasticNet models. Our interpretation of

369    AltumAge provides a detailed relationship between each of the 20,318 CpG sites and age, showing that while most

18

370 CpG sites are mostly linearly related with age, some important ones are not. Given recent advances in epigenetic

371 editing [1], finding these DNA methylation sites to delay or reverse aging may be necessary for future interventions

372 to tackle the disease. AltumAge allied with other deep learning inference methods can provide information on

373 highly interacting CpG sites. Sometimes the primary locus of an epigenetic editing intervention, given its place

374 in the genome, may be difficult to target because of the chromatin structure. Consequently, knowing secondary

375 CpG sites that affect how the CpG of interest interacts with age could guide such interventions. We show that

376 one can obtain biological hypotheses for the same from the data using AltumAge. For example, we observe

377 that cg01511567 located inside the gene SSRP1 could regulate cg10523019, which lies in RHBDD1. Analysis

378 of ChromHMM annotations shows that the top-ranking CpG sites are associated with gene regulatory regions

379 and CTCF binding sites. Finally, we highlight the age-related KEGG pathways obtained for genes with these

380 CpG sites, indicating that the model is learning valuable biological information from the data.

381 We also explore how age acceleration as determined by AltumAge has meaningful biological significance.

382 AltumAge, in contrast to Horvath's model, predicts higher age acceleration for cancer. It seems that only

383 epigenetic clocks predictive of mortality show this behavior consistently [50]. Age acceleration in tumors can

384 be thought of as a further deviation from the original state in Waddington's landscape. AltumAge predicts

385 higher age acceleration *in vitro* for cells with mitochondrial dysfunction and replicative senescence, similarly

386 to Horvath's model. More importantly, AltumAge displays a much higher correlation between cell passage

387 number and predicted age. Intriguingly as well, AltumAge does not uncover a rejuvenation event from transient

388 reprogramming [58]. This observation is possibly due to the temporary nature of the rejuvenation event, which

389 may not globally change age-related DNA methylation patterns. Since AltumAge considers a much larger portion

390 of the epigenome, it may be more resistant to detecting momentary rejuvenation.

391 In future work, it would be interesting to create a deep learning model with Illumina's EPIC array with the

392 roughly 850 thousand CpG sites to understand more deeply how genomic location can affect influence in aging.

393 In addition, by having several CpG sites in a single gene, it is also possible to better understand how methylation

394 in different positions may affect the contribution of a particular gene to the aging process. Currently, however,

395 there are only a few EPIC array data sets publicly available.

396 Overall, we have shown that deep learning represents an improvement in performance over current approaches

397 for epigenetic clocks while at the same time providing new, relevant biological insights about the aging process.

19

## Methods

### DNA methylation data sets

For model training and testing, we gathered normal tissue samples from 143 publicly available DNA methylation data sets from the Gene Expression Omnibus, Array Express, and The Cancer Genome Atlas, comprising of the platforms Illumina Infinium Human-Methylation27 and the Illumina Infinium HumanMethylation450. All selected data sets had both processed beta values and age available for all samples. Missing values per data set were imputed with a KNN imputer from `scikit-learn`. Next, the data was normalized using the beta mixture quantile normalization (BMIQ) with the optimized code from Horvath, called BMIQCalibration [3, 63]. 13 data sets contained tumor samples which were separated for later analysis. Then, each data set was split 60% for training (n = 8999) and 40% for testing (n = 6091). The within-data set split ensures the distribution of age, gender, and tissue type between training and testing sets are unbiased (Supplementary Figure S2). In the training set, the data was further randomly subdivided by data set, with 77 (n = 4339) for model selection and 76 (n = 4660) for validation. The full list of data sets used is available in the paper's GitHub repository (https://github.com/rsinghlab/AltumAge).

For twelve data sets in which gestational week was available, the encoding for age is the following:

$$y = 7 * \frac{w - 40}{365} \qquad (1)$$

where $w$ is the gestational week, and $y$ is the age in years. A gestational week below 40 would have negative age; for instance, 30 weeks would be encoded as $7 * (30 - 40)/365 = -0.192$. In the US in 2013, the average birth occurred at an estimated 38.5 weeks [64]. This number has changed slightly over time, and since preterm deliveries skew the average more than late-term births, we considered gestational week 40 as age 0 in such data sets.

For the cancer age acceleration analysis, we compared the test set of 13 data sets with the aforementioned separated cancer samples. These data sets were GSE32393, GSE37988, GSE26126, GSE63384, GSE59157, GSE32867, GSE30759, GSE31979, GSE77955, GSE52068, GSE49149, GSE39004. We further added GSE53051, which contains normal and tumor samples from five tissue types, for the analysis. It is worth noting that analyzing GSE53051 separately did not change the outcome of higher tumor age acceleration predicted with AltumAge vs. no difference with Horvath's model. In total, we compared 732 normal and 3712 cancer observations across 10 different tissue types (Figure 5).

### CpG site annotation

For the annotation of CpG sites, GENCODE and Zhou et al's annotations were used [65, 66]. 41 data sets from ENCODE with the 18-state ChromHMM information were gathered [33]: ENCFF717HFZ, ENCFF718AGZ, ENCFF371WNR, ENCFF318XQO, ENCFF340OUL, ENCFF893CAJ, ENCFF151PZS, ENCFF098CED, ENCFF273PJW, ENCFF377YFI, ENCFF773VYR, ENCFF928QES, ENCFF786HDE, ENCFF827FZN, ENCFF364PIY, ENCFF802QCI, ENCFF021NNN, ENCFF510ZEI, ENCFF175NGE, ENCFF670DBL, ENCFF825ZCZ, ENCFF912ILE, ENCFF725WBV, ENCFF829SZB, ENCFF483NRC, ENCFF717RYX, ENCFF249ZBG, ENCFF205OTD, ENCFF765OKG, ENCFF820YPQ, ENCFF685BMF, ENCFF545ZMG, ENCFF294UQS, ENCFF104ZSA, ENCFF370EGY, ENCFF860FWW, ENCFF177TTP, ENCFF151ZGD, ENCFF743GHZ, ENCFF990YHL, and ENCFF036WIO. Since AltumAge is a pan-tissue clock, the mode of each state was chosen for each CpG site.

## Model selection

Multiple machine learning models were tested in the validation set. The evaluation metrics were median absolute error (MAE), mean squared error (MSE), Pearson's correlation coefficient (R), and median error.

To validate and train the models, the beta value of each CpG site was scaled with a robust scaler which removes the median and scales according to the interquantile range. A robust scaler was chosen as opposed to a standard scaler (mean = 0, var = 1) to better resist distortions caused by outliers. In addition, only 20,318 CpG sites common to all three platforms Illumina Infinium HumanMethylation27, Illumina Infinium HumanMethylation450, Infinium Methylation EPIC were chosen as features.

The non-neural network models trained with `scikit-learn` were support vector regression (with an RBF kernel) and random forest with the standard hyperparameters. ElasticNet, trained with `glmnet`, used the built-in $\lambda$ optimization with parameters alpha = 0.5 and n_splits = 10. Moreover, for ElasticNet, Horvath's age transformation was used [3].

To select the best performing neural network with `tensorflow`, we conducted a grid search with the following hyperparameters: number of hidden layers (2, 5, or 8), number of neurons per dense layer (32 or 64), activity and kernel regularization coefficients (0, 0.0034, or 0.0132), dropout (0 or 0.1), Gaussian dropout (0 or 0.1), batch normalization (yes or no), activation function (ReLU or SeLU), and learning rate (0.0002, 0.0005, or 0.001). The following parameters were held constant: optimizer (Adam), batch size (256), number of epochs (300), loss function (MSE), and learning rate decay by a factor of 0.2 after a 30-epoch plateau in the training loss. The weights with the lowest training loss were chosen. After selecting the best hyperparameters, we trained the neural network with adversarial regularization with `neural_structured_learning` with multiplier=0.05, adv_step_size=0.005.

We dubbed the best performing deep neural network as AltumAge. It consists of 5 hidden layers, 32 neurons per layer, activity and kernel regularization coefficients of 0.0034, no dropout, gaussian dropout of 0.1, with batch normalization, SeLU activation, and learning rate of 0.001. AltumAge was also tested in the validation set with a smaller set of features using the CpG sites selected from the ElasticNet.

To compare our deep learning approach with other state-of-the-art neural networks, we tried TabNet, an attentive interpretable tabular learning method [17]. Similarly, TabNet was trained for 300 epochs.

The results for the validation set with the full list of models, including the replication of Horvath's model [3], is in Supplementary Table S1. Support vector regression was by far the worst performer (MAE = 14.229, MSE = 458.956), followed by random forest (MAE = 6.833, MSE = 165.354). All other models displayed R > 0.9, with AltumAge having the lowest MAE (3.563) and MSE (57.071).

## SHAP and DeepPINK

To obtain the SHAP values for AltumAge, the function `GradientExplainer` from `shap` was used on the test set. For the DeepPINK importance values and feature selection, the standard architecture and number of epochs was used [26]. To create the knockoff features for DeepPINK, the function `knockoff.filter` from the R 4.0.2 package `knockoff` version 0.3.3 was used with the importance statistic based on the square-root lasso.

Both SHAP and DeepPINK importance values were normalized so that their sum would equal to 100. Each importance value thus represents a percent contribution of a certain feature.

## Statistical Analysis

All statistical tests were conducted with packages `scikit-learn`, `statsmodel`, or `scipy`. Tests that were one-sided were explicitly mentioned in the main text; all others were two-sided.

To assess the performance of the models, we used median absolute error (MAE), mean squared error (MSE), Pearson's correlation coefficient (R), and median error.

## Code Availability

Detailed instructions on how to run AltumAge can be found in the paper's GitHub repository (https://github.com/rsinghlab/AltumAge). All code was run with Python (3.9.1) and packages `scikit-learn` (0.24.2), `pandas` (1.3.0), `numpy` (1.19.5), `glmnet` (1.1), `tensorflow` (2.5.0), `neural_structured_learning` (1.3.1), `statsmodel` (0.10.2), `scipy` (1.7.0), `shap` (0.39.0).

## Data Availability

The list of all the data sets used, a summary of the results per data set, and detailed instructions to run AltumAge can be found in the paper's GitHub repository (https://github.com/rsinghlab/AltumAge). The GitHub also links to a Google Drive where our gathered DNA methylation data is publicly available.

## Author Contributions

L.P.L.C conceived of the presented idea. R.S and L.P.L.C designed the methodology and the experiments. L.P.L.C conducted all the experiments. L.R.L assisted with the analysis and biological interpretation of the results. All authors discussed the results and contributed to the final manuscript.

## Funding

## Competing Interests Statement

The authors declare that they have no conflict of interest.

## References

[1]  James K. Nuñez et al. "Genome-Wide Programmable Transcriptional Memory by CRISPR-Based Epigenome Editing". English. In: *Cell* 184.9 (Apr. 2021), 2503–2519.e17. ISSN: 0092-8674, 1097-4172. DOI: 10.1016/j.cell.2021.03.025.

[2] Gregory Hannum et al. "Genome-Wide Methylation Profiles Reveal Quantitative Views of Human Aging Rates". In: *Molecular cell* 49.2 (Jan. 2013), pp. 359–367. ISSN: 1097-2765. DOI: `10.1016/j.molcel.2012.10.016`.

[3] Steve Horvath. "DNA Methylation Age of Human Tissues and Cell Types". In: *Genome Biology* 14.10 (Dec. 2013), p. 3156. ISSN: 1474-760X. DOI: `10.1186/gb-2013-14-10-r115`.

[4] Gregory M. Fahy et al. "Reversal of Epigenetic Aging and Immunosenescent Trends in Humans". en. In: *Aging Cell* 18.6 (2019), e13028. ISSN: 1474-9726. DOI: `10.1111/acel.13028`.

[5] Li Chen et al. "Effects of Vitamin D3 Supplementation on Epigenetic Aging in Overweight and Obese African Americans With Suboptimal Vitamin D Status: A Randomized Clinical Trial". In: *The Journals of Gerontology Series A: Biological Sciences and Medical Sciences* 74.1 (Jan. 2019), pp. 91–98. ISSN: 1079-5006. DOI: `10.1093/gerona/gly223`.

[6] Nelly Olova et al. "Partial Reprogramming Induces a Steady Decline in Epigenetic Age before Loss of Somatic Identity". In: *Aging Cell* 18.1 (Feb. 2019). ISSN: 1474-9718. DOI: `10.1111/acel.12877`.

[7] Kara N. Fitzgerald et al. "Potential Reversal of Epigenetic Age Using a Diet and Lifestyle Intervention: A Pilot Randomized Clinical Trial". en. In: *Aging* (Mar. 2021). ISSN: 1945-4589. DOI: `10.18632/aging.202913`.

[8] Hui Zou and Trevor Hastie. "Regularization and Variable Selection via the Elastic Net". en. In: *Journal of the Royal Statistical Society: Series B (Statistical Methodology)* 67.2 (Apr. 2005), pp. 301–320. ISSN: 1369-7412, 1467-9868. DOI: `10.1111/j.1467-9868.2005.00503.x`.

[9] Morgan E. Levine et al. "An Epigenetic Biomarker of Aging for Lifespan and Healthspan". In: *Aging (Albany NY)* 10.4 (Apr. 2018), pp. 573–591. ISSN: 1945-4589. DOI: `10.18632/aging.101414`.

[10] Ake T. Lu et al. "DNA Methylation GrimAge Strongly Predicts Lifespan and Healthspan". In: *Aging (Albany NY)* 11.2 (Jan. 2019), pp. 303–327. ISSN: 1945-4589. DOI: `10.18632/aging.101684`.

[11] Michael J. Thompson et al. "A Multi-Tissue Full Lifespan Epigenetic Clock for Mice". In: *Aging (Albany NY)* 10.10 (Oct. 2018), pp. 2832–2854. ISSN: 1945-4589. DOI: `10.18632/aging.101590`.

[12] Steve Horvath et al. "Reversing Age: Dual Species Measurement of Epigenetic Age with a Single Clock". en. In: *bioRxiv* (May 2020), p. 2020.05.07.082917. DOI: `10.1101/2020.05.07.082917`.

[13] V. J. Sugrue et al. "Castration Delays Epigenetic Aging and Feminises DNA Methylation at Androgen-Regulated Loci". en. In: *bioRxiv* (Nov. 2020), p. 2020.11.16.385369. DOI: `10.1101/2020.11.16.385369`.

[14]   Polina Mamoshina Fedor Galkin and Polina Mamoshina Fedor Galkin. "DeepMAge: A Methylation Aging Clock Developed with Deep Learning". en. In: *Aging and disease* (), p. 0. ISSN: 2152-5250. DOI: 10.14336/AD.2020.1202.

[15]   Joshua J. Levy et al. "MethylNet: An Automated and Modular Deep Learning Approach for DNA Methylation Analysis". In: *BMC Bioinformatics* 21.1 (Mar. 2020), p. 108. ISSN: 1471-2105. DOI: 10.1186/s12859-020-3443-8.

[16]   Scott M. Lundberg and Su-In Lee. "A Unified Approach to Interpreting Model Predictions". en. In: *Advances in Neural Information Processing Systems* 30 (2017), pp. 4765–4774.

[17]   Sercan O Arık and Tomas Pfister. "Tabnet: Attentive interpretable tabular learning". In: *arXiv* (2020).

[18]   Arlind Kadra et al. "Regularization is all you Need: Simple Neural Nets can Excel on Tabular Data". In: *arXiv preprint arXiv:2106.11189* (2021).

[19]   Louis Y. El Khoury et al. "Systematic Underestimation of the Epigenetic Clock and Age Acceleration in Older Subjects". In: *Genome Biology* 20.1 (Dec. 2019), p. 283. ISSN: 1474-760X. DOI: 10.1186/s13059-019-1810-4.

[20]   Lauren N Booth and Anne Brunet. "The aging epigenome". In: *Molecular cell* 62.5 (2016), pp. 728–744.

[21]   Ian J Goodfellow, Jonathon Shlens, and Christian Szegedy. "Explaining and harnessing adversarial examples". In: *arXiv preprint arXiv:1412.6572* (2014).

[22]   Ramprasaath R Selvaraju et al. "Grad-cam: Visual explanations from deep networks via gradient-based localization". In: *Proceedings of the IEEE international conference on computer vision*. 2017, pp. 618–626.

[23]   Mukund Sundararajan, Ankur Taly, and Qiqi Yan. "Axiomatic attribution for deep networks". In: *arXiv preprint arXiv:1703.01365* (2017).

[24]   Daniel Smilkov et al. "Smoothgrad: removing noise by adding noise". In: *arXiv preprint arXiv:1706.03825* (2017).

[25]   Dzmitry Bahdanau, Kyunghyun Cho, and Yoshua Bengio. "Neural machine translation by jointly learning to align and translate". In: *arXiv preprint arXiv:1409.0473* (2014).

[26]   Yang Lu et al. "DeepPINK: Reproducible Feature Selection in Deep Neural Networks". en. In: *Advances in Neural Information Processing Systems* 31 (2018), pp. 8676–8686.

[27]   Gilad Fuchs et al. "4sUDRB-seq: measuring genomewide transcriptional elongation rates and initiation frequencies within cells". In: *Genome biology* 15.5 (2014), pp. 1–11.

24

[28] Yang Han et al. "New targeted approaches for epigenetic age predictions". In: *BMC biology* 18.1 (2020), pp. 1–15.

[29] Yunzhang Wang et al. "Epigenetic influences on aging: a longitudinal genome-wide methylation study in old Swedish twins". In: *Epigenetics* 13.9 (2018), pp. 975–987.

[30] Tian Yuan et al. "An integrative multi-scale analysis of the dynamic DNA methylation landscape in aging". In: *PLoS genetics* 11.2 (2015), e1004996.

[31] Lucas Paulo de Lima Camillo and Robert B. A. Quinlan. "A Ride through the Epigenetic Landscape: Aging Reversal by Reprogramming". en. In: *GeroScience* (Apr. 2021). ISSN: 2509-2723. DOI: 10.1007/s11357-021-00358-6.

[32] Jason Ernst and Manolis Kellis. "ChromHMM: Automating Chromatin-State Discovery and Characterization". en. In: *Nature Methods* 9.3 (Mar. 2012), pp. 215–216. ISSN: 1548-7105. DOI: 10.1038/nmeth.1906.

[33] Carrie A. Davis et al. "The Encyclopedia of DNA Elements (ENCODE): Data Portal Update". eng. In: *Nucleic Acids Research* 46.D1 (Jan. 2018), pp. D794–D801. ISSN: 1362-4962. DOI: 10.1093/nar/gkx1081.

[34] Han Chen et al. "Fast-evolving human-specific neural enhancers are associated with aging-related diseases". In: *Cell systems* 6.5 (2018), pp. 604–611.

[35] Lijun Zhao et al. "Sirtuins and Their Biological Relevance in Aging and Age-Related Diseases". In: *Aging and Disease* 11.4 (July 2020), pp. 927–945. ISSN: 2152-5250. DOI: 10.14336/AD.2019.0820.

[36] Thomas Weichhart. "mTOR as Regulator of Lifespan, Aging and Cellular Senescence". In: *Gerontology* 64.2 (2018), pp. 127–134. ISSN: 0304-324X. DOI: 10.1159/000484629.

[37] Kristopher Burkewitz, Yue Zhang, and William B. Mair. "AMPK at the Nexus of Energetics and Aging". In: *Cell metabolism* 20.1 (July 2014), pp. 10–25. ISSN: 1550-4131. DOI: 10.1016/j.cmet.2014.03.002.

[38] Andrew D. Rouillard et al. "The Harmonizome: A Collection of Processed data sets Gathered to Serve and Mine Knowledge about Genes and Proteins". In: *Database* 2016.baw100 (Jan. 2016). ISSN: 1758-0463. DOI: 10.1093/database/baw100.

[39] Minoru Kanehisa and Yoko Sato. "KEGG Mapper for Inferring Cellular Functions from Protein Sequences". eng. In: *Protein Science: A Publication of the Protein Society* 29.1 (Jan. 2020), pp. 28–35. ISSN: 1469-896X. DOI: 10.1002/pro.3711.

[40] Minoru Kanehisa and Yoko Sato. "KEGG Mapper for inferring cellular functions from protein sequences". In: *Protein Science* 29.1 (2020), pp. 28–35.

[41] Steve Horvath et al. "Obesity accelerates epigenetic aging of human liver". In: *Proceedings of the National Academy of Sciences* 111.43 (2014), pp. 15538–15543.

[42] Morgan E Levine et al. "Menopause accelerates biological aging". In: *Proceedings of the National Academy of Sciences* 113.33 (2016), pp. 9327–9332.

[43] Chanachai Sae-Lee et al. "Dietary intervention modifies DNA methylation age assessed by the epigenetic clock". In: *Molecular nutrition & food research* 62.23 (2018), p. 1800092.

[44] Steve Horvath et al. "An epigenetic clock analysis of race/ethnicity, sex, and coronary heart disease". In: *Genome biology* 17.1 (2016), pp. 1–23.

[45] Klára Marečková et al. "Epigenetic clock as a correlate of anxiety". In: *NeuroImage: Clinical* 28 (2020), p. 102458.

[46] Giovanni Fiorito et al. "Socioeconomic position, lifestyle habits and biomarkers of epigenetic aging: a multi-cohort analysis". In: *Aging (Albany NY)* 11.7 (2019), p. 2045.

[47] Yinan Zheng et al. "Blood epigenetic age may predict cancer incidence and mortality". In: *EBioMedicine* 5 (2016), pp. 68–73.

[48] Srikant Ambatipudi et al. "DNA methylome analysis identifies accelerated epigenetic ageing associated with postmenopausal breast cancer susceptibility". In: *European journal of cancer* 75 (2017), pp. 299–307.

[49] Morgan E Levine et al. "DNA methylation age of blood predicts future onset of lung cancer in the women's health initiative". In: *Aging (Albany NY)* 7.9 (2015), p. 690.

[50] Zuyun Liu et al. "Underlying features of epigenetic aging clocks in vivo and in vitro". In: *Aging Cell* 19.10 (2020), e13229.

[51] Wenbing Xie et al. "DNA methylation patterns separate senescence from transformation potential and indicate cancer risk". In: *Cancer cell* 33.2 (2018), pp. 309–321.

[52] Kristopher L Nazor et al. "Recurrent variations in DNA methylation in human pluripotent stem cells and their differentiated derivatives". In: *Cell stem cell* 10.5 (2012), pp. 620–634.

[53] Oswaldo A Lozoya et al. "Mitochondrial nicotinamide adenine dinucleotide reduced (NADH) oxidation links the tricarboxylic acid (TCA) cycle with methionine metabolism and nuclear DNA methylation". In: *PLoS biology* 16.4 (2018), e2005707.

26

[54] Carlos de Torre-Minguela, Pablo Mesa del Castillo, and Pablo Pelegrin. "The NLRP3 and pyrin inflammasomes: implications in the pathophysiology of autoinflammatory diseases". In: *Frontiers in immunology* 8 (2017), p. 43.

[55] Guangxun Meng et al. "A mutation in the Nlrp3 gene causing inflammasome hyperactivation potentiates Th17 cell-dominant immune responses". In: *Immunity* 30.6 (2009), pp. 860–874.

[56] Jessica Carriere, Andrea Dorfleutner, and Christian Stehlik. "NLRP7: From Inflammasome Regulation to Human Disease". In: *Immunology* (2020).

[57] Sangeetha Mahadevan et al. "NLRP7 affects trophoblast lineage differentiation, binds to overexpressed YY1 and alters CpG methylation". In: *Human molecular genetics* 23.3 (2014), pp. 706–716.

[58] Tapash Jay Sarkar et al. "Transient non-integrative expression of nuclear reprogramming factors promotes multifaceted amelioration of aging in human cells". In: *Nature communications* 11.1 (2020), pp. 1–12.

[59] Alejandro Ocampo et al. "In vivo amelioration of age-associated hallmarks by partial reprogramming". In: *Cell* 167.7 (2016), pp. 1719–1733.

[60] Maria Manukyan and Prim B Singh. "Epigenome rejuvenation: HP1$\beta$ mobility as a measure of pluripotent and senescent chromatin ground states". In: *Scientific reports* 4.1 (2014), pp. 1–8.

[61] Li Guo et al. "Generation of induced progenitor-like cells from mature epithelial cells using interrupted reprogramming". In: *Stem cell reports* 9.6 (2017), pp. 1780–1795.

[62] Steve Horvath and Kenneth Raj. "DNA Methylation-Based Biomarkers and the Epigenetic Clock Theory of Ageing". en. In: *Nature Reviews Genetics* 19.6 (June 2018), pp. 371–384. ISSN: 1471-0064. DOI: 10.1038/s41576-018-0004-3.

[63] Andrew E. Teschendorff et al. "A Beta-Mixture Quantile Normalization Method for Correcting Probe Design Bias in Illumina Infinium 450 k DNA Methylation Data". In: *Bioinformatics* 29.2 (Jan. 2013), pp. 189–196. ISSN: 1367-4803. DOI: 10.1093/bioinformatics/bts680.

[64] "National Vital Statistics Reports, Volume 64, Number 5, (06/01/2015)". en. In: (), p. 20.

[65] Adam Frankish et al. "GENCODE Reference Annotation for the Human and Mouse Genomes". eng. In: *Nucleic Acids Research* 47.D1 (Jan. 2019), pp. D766–D773. ISSN: 1362-4962. DOI: 10.1093/nar/gky955.

[66] Wanding Zhou, Peter W. Laird, and Hui Shen. "Comprehensive Characterization, Annotation and Innovative Use of Infinium DNA Methylation BeadChip Probes". In: *Nucleic Acids Research* 45.4 (Feb. 2017), e22–e22. ISSN: 0305-1048. DOI: 10.1093/nar/gkw967.

# Supplementary Information

## DeepPINK

To support the results obtained by SHAP, we also applied another method of determining feature importance called DeepPINK [26]. It works by comparing the original features with fake features. The knockoff features can be generated in many different ways, as long as they simulate the original data structure but are not related to the output. DeepPINK contrasts the relevance of the fake features against the regular input features to determine which ones are truly related to the output. It can also be used for feature selection with a controllable false discovery rate (FDR). It is worth highlighting the difficulty in feature selection in DNA methylation data. Most experiments have a couple dozen or a couple hundred samples. Depending on the type of platform used, the number of beta values for the CpG sites analyzed can vary from around 27 thousand to around 850 thousand. DeepPINK, even with a high FDR of 0.5, only selected 78 features. The fact that other sets of CpG sites unrelated to Horvath's 353 also perform similarly well emphasizes the difficulty in finding the "true" age-related CpG sites.

**AltumAge captures relevant age-related CpG-CpG interactions** The top 9 most important CpG sites according to SHAP account for 9.54% of total DeepPINK model importance.

**Characterization of CpG sites by model interpretation**. For the CTCF binding site analysis, the top 1000 CpG sites comprises 47.3% of DeepPINK importance. For the ChromHMM analysis, CpG importance values are also impacted by ChromHMM state for DeepPINK (Kruskal-Wallis H-test p-value = 2.982e-05). The chromatin state with the highest DeepPINK normalized median importance was heterochromatin (DeepPINK importance = 2.47e-14%, top 66th percentile of all CpG sites). Despite there being only 29 CpG sites characterized as heterochromatic, this result emphasizes the importance of chromatin packing with aging, as it is related to genome stability and maintenance.

**Aging-related pathways**. None of the CpG sites in SIRT genes appear very relevant for DeepPINK. cg21770145, located in SIRT7, accounts for 7.89e-12% of total DeepPINK importance and ranks 1342, with the highest SIRT DeepPINK importance value. For the mTOR pathway, cg05546044, located in MAPK1, has the highest DeepPINK importance of 0.029%, ranking 233. mTOR was not particularly relevant, with its most important CpG site being cg07029998 (DeepPINK importance = 1.12e-12%, rank 2459). All AMPK-related CpG sites had low (less than 10e-13%) DeepPINK importance values.

## Tables and Figures

28

Table S1: Evaluation metrics for all models in the validation set. The median absolute error (MAE) and the median error are in units of year, while the mean squared error (MSE) is in units of year-squared.

| Model | CpGs | MAE | MSE | R | Median Error |
|---|---|---|---|---|---|
| AltumAge | 20318 | **3.563** | **57.071** | **0.954** | -0.465 |
| AltumAge with ElasticNet CpGs | 653 | 3.600 | 65.642 | 0.947 | -0.369 |
| ElasticNet | 653 | 3.674 | 73.323 | 0.942 | 0.110 |
| TabNet | 20318 | 4.172 | 75.149 | 0.939 | 0.178 |
| Random Forest | 20318 | 6.833 | 165.354 | 0.861 | **0.091** |
| Support Vector Regression | 20318 | 14.229 | 458.956 | 0.576 | -4.853 |

Table S2: List of ChromHMM states by ChromHMM state ID.

| ChromHMM state ID | ChromHMM state |
|---|---|
| 1 | Active TSS |
| 2 | Flanking TSS |
| 3 | Flanking TSS Upstream |
| 4 | Flanking TSS Downstream |
| 5 | Strong transcription |
| 6 | Weak transcription |
| 7 | Genic enhancer1 |
| 8 | Genic enhancer2 |
| 9 | Active Enhancer 1 |
| 10 | Active Enhancer 2 |
| 11 | Weak Enhancer |
| 12 | ZNF genes and repeats |
| 13 | Heterochromatin |
| 14 | Bivalent/Poised TSS |
| 15 | Bivalent Enhancer |
| 16 | Repressed PolyComb |
| 17 | Weak Repressed PolyComb |
| 18 | Quiescent/Low |
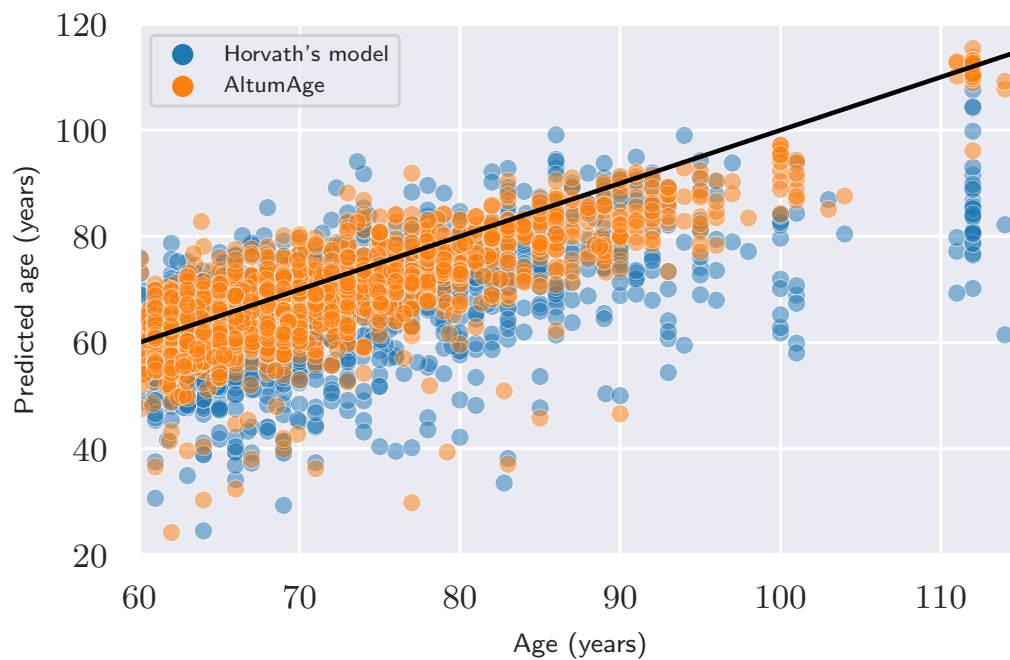
Figure S1: Scatter plot showing the improved performance of AltumAge in comparison to Horvath's 2013 model for older ages. The black line represents the location where the predicted age equals the real age. AltumAge's predictions are generally closer to the black line. Horvath's predictions tends to give lower performance in higher ages.
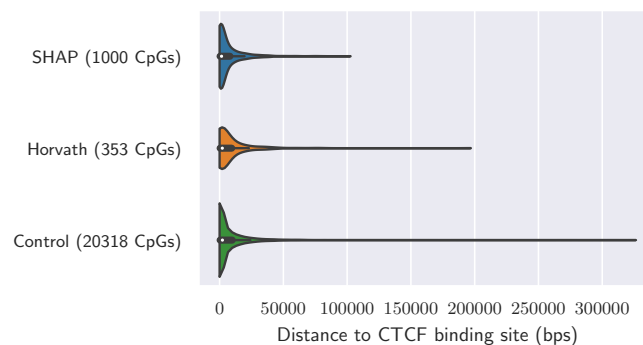
(a)

(b)

(c)

Figure S2: Distribution of age, gender, and tissue type in both training and testing sets. The distributions of age (a) and gender (b) are virtually identical between the two sets. Similarly with the distribution of tissue type (c) in training (left) and testing (right).



Figure S3: Histogram of the normalized importance values of all AltumAge CpG sites according to SHAP. The red line represents the threshold for the top nine CpG sites. These have a much higher importance than most other CpG sites.

31

Figure S4: Violin plot showing that the top 1000 CpG sites according to SHAP are closer to CTCF binding sites than the 20,318 control CpG sites. Horvath's CpG sites are not statistically significantly different from the control.
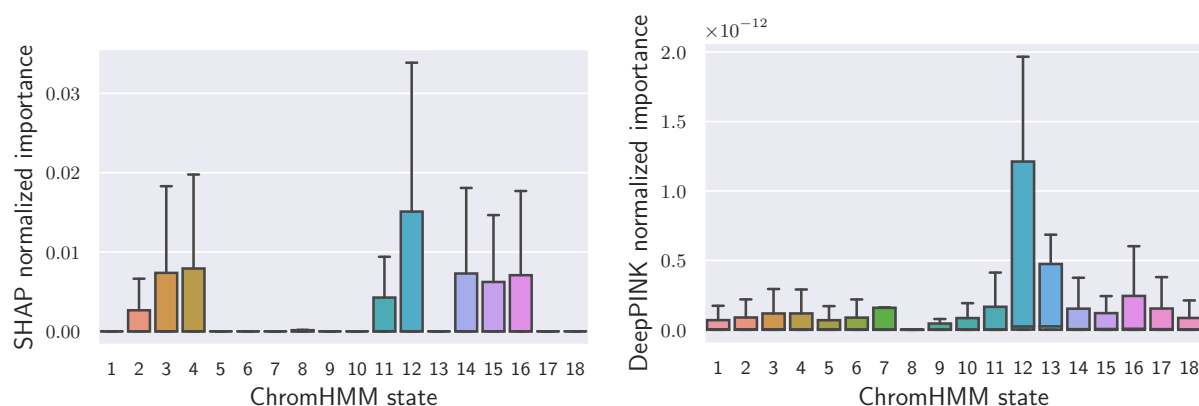


Figure S5: Box plots of SHAP and DeepPINK normalized importance values by ChromHMM state. Outliers were removed for better figure visualization. No specific ChromHMM state stands out in importance.
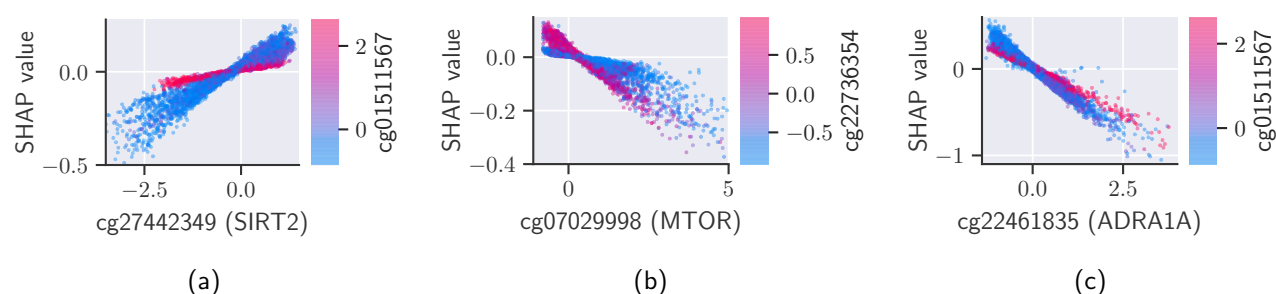


Figure S6: SHAP dependence plots of three CpG sites in SIRT2, mTOR, and ADRA1A. The x-axis shows the standardized beta values for each specific CpG site; the y-axis, its SHAP value, and the coloring scheme, the scaled beta values for the CpG site with the highest interaction. These are the most important CpG sites according to SHAP for AltumAge in the SIRT and mTOR pathways.
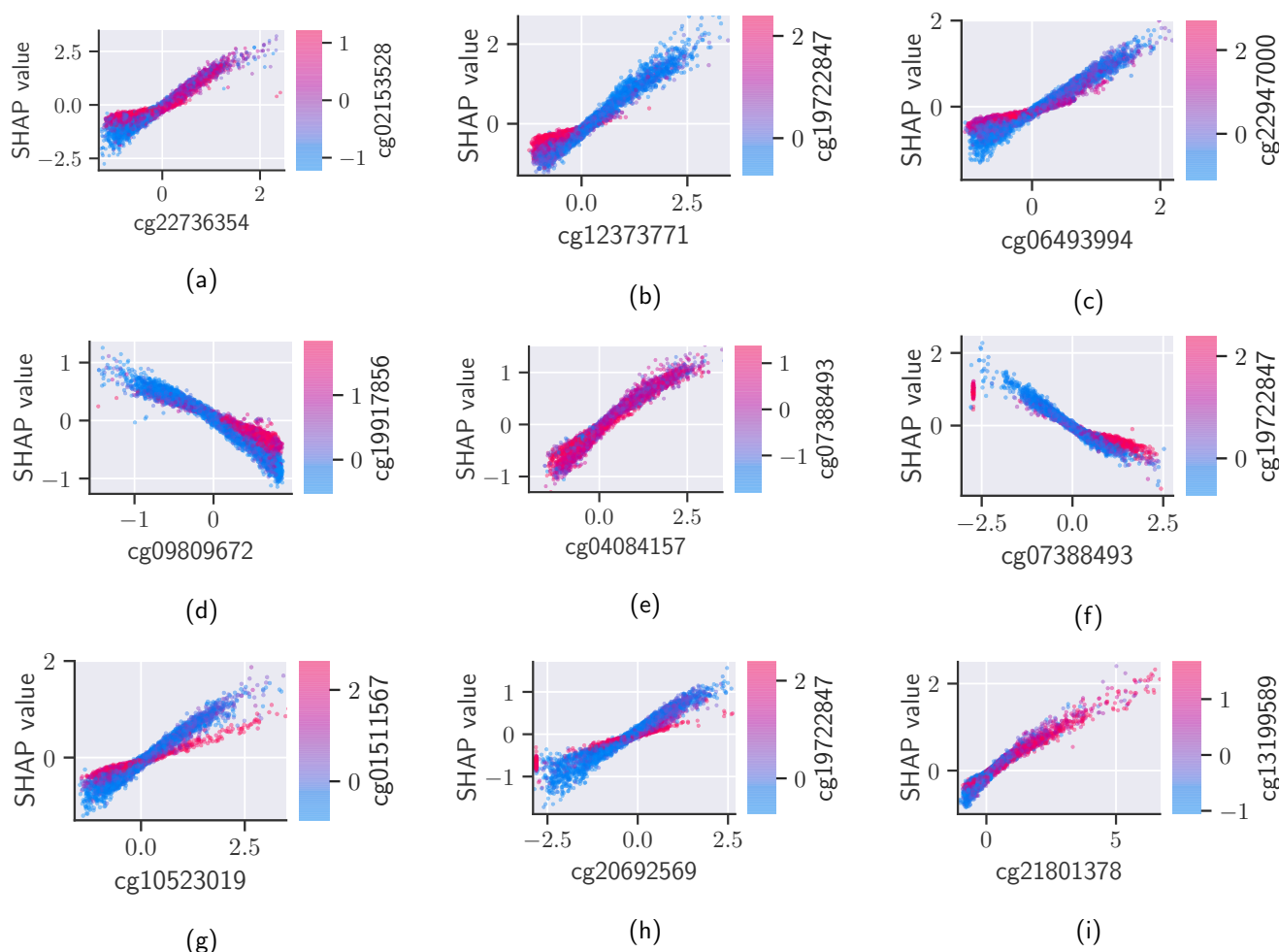
Figure S7: Dependence plots of the nine most important CpG sites (a-i) in AltumAge based on SHAP values. They are ordered from top left to bottom right in terms of importance. The x-axis shows the scaled beta values for each specific CpG site; the y-axis, its SHAP value, and the coloring scheme, the scaled beta values for the CpG site with the highest interaction. The effect of a specific CpG site on the predicted age can vary based on a secondary CpG site.
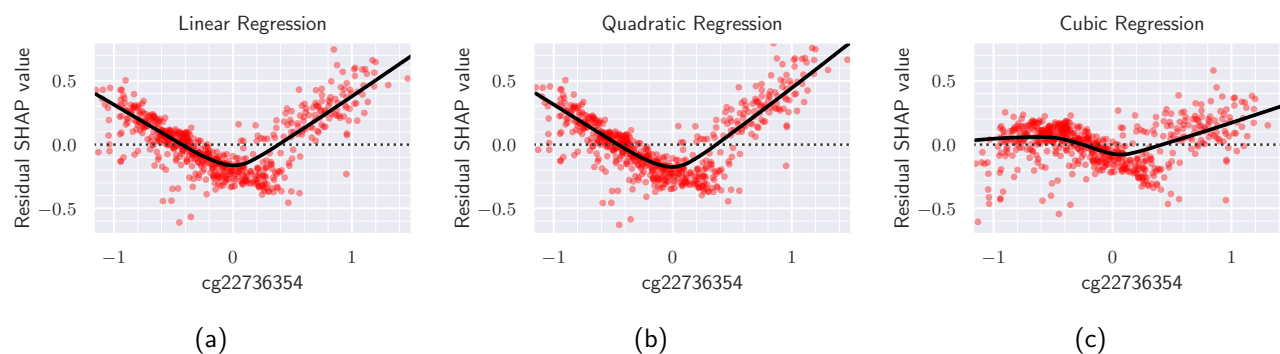


Figure S8: Residual plots of cg22736354 by order of regression. A linear regression (a) underestimates around the boundaries and underestimates in the middle, demonstrating the non-linear relationship. The same occurs with a quadratic regression (b). When the order is increased to three, the cubic regression (c) takes the non-linearity better into account.
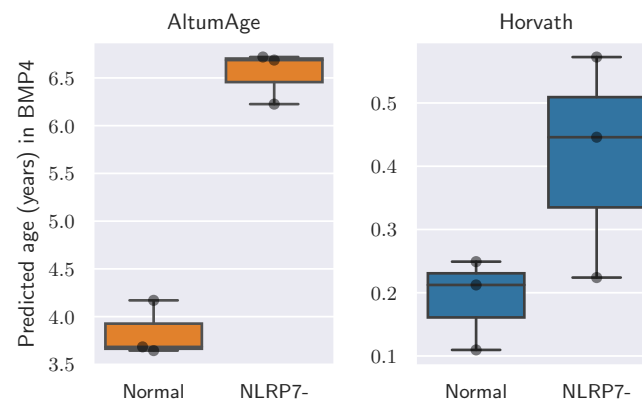
Figure S9: Box plots showing predicted age of H9 ESCs with NLRP7 knockdown (NLRP7-) or control (Normal) in BMP4 differentiating medium.